Accepted by ApJ.

Periodicities in Solar Flare Occurrence: Analysis of Cycles 19–23

T. Bai

Stanford University, Stanford, CA 94305

bai@quake.stanford.edu

ABSTRACT

Mid-range periodicities in solar flare occurrence have been analyzed with new methods for cycles 19–23. During cycle 23, periodicities of 129-d and 33.5-d were in operation. Five episodes of high activity occurred periodically with the 129-d period. The 33.5-d periodicity mainly operated for energetic flares. Results for cycles 19–21 are generally in agreement with previous analyses. For cycle 19, the 51-d periodicity is confirmed to be statistically significant. In the spectrum for cycle 20, two peaks are found at 84 d and 129 d. The 129-d periodicity was in operation for 8 cycles of 129 d. The 153-d periodicity, which operated during cycle 21, was more effective for modulating occurrence rates of energetic flares than those of less energetic flares. No statistically significant periodicities are found from occurrence rates of energetic flares ($\geq$M1.0) of cycle 22. In the power spectra of major flare occurrence times for the time intervals analyzed by Ozguc & Atac and Bai, strongest peaks are found at 73 d, 76 d, and 51 d, in agreement with their results, but these periodicities are not statistically significant. It is interesting that the periods of 51, 129, and 153 days are very close to integral multiples of 25.5 days.

Subject headings: Sun: activity—Sun: flares—Sun: periodicity

April 8, 2003

1. Introduction

As a long-term periodicity, the Sun exhibits the 11-year sunspot cycle, which has been known for a long time. For short terms, the Sun often exhibits 27-d and 13.5-d periodicities, which tell more about spatial organization of the solar activity than its temporal organization. The regime between these extremes of time scales (between 27 d and 11 y) is called the "mid range."

Relatively recently, periodicities in this mid range have been explored, starting with the discovery of a 153-d periodicity in γ-ray flare occurrence (Rieger et al. 1984). Since then, many researchers investigated mid-range periodicities, using various solar activity indicators.

First of all, regardless of selection criteria, flare occurrence rates of solar cycle 21 all exhibited the 153-d periodicity: soft X-ray peak flux (Rieger et al. 1984); hard X-ray peak rate (Dennis 1985; Bai & Sturrock 1987; Verma & Joshi 1987); Hα importance (Ichimoto et al. 1985); Hα flare index (Ozguc & Atac 1989); 10-cm radio peak flux (Kile & Cliver 1991); production of solar energetic protons (Bai & Cliver 1990; Gabriel et al. 1990); production of energetic electrons in interplanetary space (Dröge et al. 1990).

Many researchers studied periodicities in sunspot areas and numbers. Analyses of sunspot areas of recent cycles generally agree that the periodicity near 154 days operated during cycles 19–21 (Lean & Brueckner 1989; Lean 1990; Oliver et al. 1998; Krivova & Solanki 2002), and this periodicity was strongest during cycle 19 and weakest during cycle 20 (Oliver et al. 1998; Krivova & Solanki 2002). This periodicity was also detected from data of earlier times than cycle 19: cycle 2 (Ballester et al. 1999); cycles 16–18 (Carbonell & Ballester 1992; Oliver et al. 1998; Ballester et al. 1999; Krivova & Solanki 2002), but not cycles 12-15 (Carbonell & Ballester 1992). In addition to the 154-d periodicity, Pap et al. (1990) discovered a 51-d periodicity in active sunspot areas (areas of growing sunspot groups) of cycle 21. Results of periodicity analyses of sunspot numbers generally agree with the results of sunspot area analyses (Lean & Brueckner 1989; Krivova & Solanki 2002), but Verma & Joshi (1987), for some reason, did not detect the 154-d periodicity from sunspot numbers of cycle 21.

Analysis of flare data of cycles 19 and 20 found other periodicities: 51-d period in flares selected by CFI(comprehensive flare index) during cycle 19 (Bai 1987), 78-d period in flares selected by microwave-peak flux during cycle 20 (Bogart & Bai 1985), 127-d period in flares selected by CFI and flares selected by 10-cm radio peak flux, respectively, during cycle 20 (Bai & Sturrock 1991; Kile & Cliver 1991), 84-d period in CFI-selected flares during cycle 20 (Bai 1992b), and the same periodicity in flares selected by peak soft X-ray flux for the 1970–1982 interval (Landscheidt 1986). Bai & Sturrock (1991) noticed that, except for

the 84-d periodicity, other periodicities (51, 78, 127, and 153 d) have periods very close to integral multiples of 25.8 d.

Although some papers reported detection of the 153-d periodicity in flare occurrence of earlier cycles than cycle 21, only statistically significant detections seem to come form flares associated with solar energetic protons (Bai & Cliver 1990; Gabriel et al. 1990).

It is important to detect mid-range flare periodicities and to calculate accurately their statistical significances because flare periodicities can provide information on properties of the Sun. In this paper I introduce new methods of flare periodicity analysis, and apply them to flares of cycles 19–23. It is appropriate time to find out which mid-range periodicities have been in operation during cycle 23 because about two years has passed since its maximum. Flare periodicities in earlier cycles (19–22) have been studied by many authors, but it seems necessary reanalyze them with the same methods so that we can compare statistical significances of several periodicities analyzed previously with different methods.

The plan of the paper is as follows. In §2.1, I describe data to be analyzed in this paper. In §2.2, after discussing why the conventional Fourier analysis is not appropriate for studying periodicities in flare occurrence, I introduce new methods for this. In §3, I apply them to analysis of periodicities in occurrence times of major flares of solar cycles 19–23. Summary and conclusions are given in §4.

2. Data and Analysis Methods

2.1. Data to be analyzed

For periodicity analysis, ideally we need lists of flares detected by the same detectors. For cycle 21, the γ-ray spectrometer (GRS) and the hard X-ray burst spectrometer (HXRBS) aboard *SMM* provided good flare lists, but it ceased to operate in November 1989. The soft X-ray detector aboard GOES (*Geostationary Operational Environmental Satellite*) provides excellent flare data since 1976. For the period from January 1955 to December 1979, Dodson & Hedeman (1971, 1975, 1981) provide lists of important flares with indices in the following five aspects of flares: Hα importance, ionizing radiation, magnitude of 10-cm radio flux, dynamic radio spectrum, and magnitude of $\sim$ 200 MHz flux. Observatories detecting these aspects did not remain the same, but more observatories were added as time passed. In spite of this, the flare lists of Dodson & Hedeman (1971, 1975, 1981) will not adversely affect mid-range periodicities because the observatories were not added at regular time intervals. The sum of these indices of a flare is defined as its CFI (comprehensive flare index).

For cycle 19, flares with CFI ≥ 6 are selected as Bai (1987) did. For cycle 20, flares with CFI ≥ 7 are selected as Bai (1992b) did. For cycles 21–23, lists of flares with GOES X-ray classes $\geq$ M1.0 are compiled and flares with various X-ray thresholds are selected for analysis. (GOES flare data are available from the website www.ngdc.noaa.gov/stp/SOLAR/solar.html.) For cycle 21, flares detected by the gamma ray spectrometer aboard the *Solar Maximum Mission (SMM)* are analyzed for comparison.

2.2. The Scargle periodogram

To study periodicity in a regular time series $X_j = X(t_j)$, a series of measurements made at times t_j separated by regular intervals, one often uses a Fourier spectral analysis. For an irregular time series, Scargle (1982) developed a periodogram calculated by the following equation.

$$P_x(\nu) = \frac{1}{2}\left\{ \frac{\left[\sum_{j=1}^{N} X_j \cos 2\pi\nu(t_j-\tau)\right]^2}{\sum_{j=1}^{N}\cos^2 2\pi\nu(t_j-\tau)} + \frac{\left[\sum_{j=1}^{N} X_j \sin 2\pi\nu(t_j-\tau)\right]^2}{\sum_{j=1}^{N}\sin^2 2\pi\nu(t_j-\tau)} \right\} \qquad (1)$$

where the relation $\tan 4\pi\nu\tau = \left(\sum_{j=1}^{N}\sin 4\pi\nu t_j\right) / \left(\sum_{j=1}^{N}\cos 4\pi\nu t_j\right)$ defines τ.

For this periodogram, the probability that the value P_x is greater than z by chance is given by $Pr(P_x \geq z) = \exp(-z)$, if a time series X_j satisfies the following three conditions. (1) The mean of the time series is zero. (2) Its standard deviation is 1. (3) Each element of the time series is statistically independent Gaussian noise.

In order to study mid-range periodicities of flare occurrence, one can use daily numbers of flares as a time series. By subtracting the mean from the time series, we can make the time series meet the first condition. Then, by dividing it by its standard deviation, we can make it satisfy the second condition. However, daily flare occurrences are not statistically independent. If flare activity is high on a certain day, we can expect flare activity to be high for the next several days. By taking weekly flare numbers as a time series, we can avoid this problem, but we degrade time information. Some researchers made a Fourier spectral analysis of daily flare numbers and normalized the result by dividing by a constant normalization factor. However, as will be shown in this paper, the normalization factor varies with frequency.

2.3. The Rayleigh analysis and its normalization

In flare data, we have a series of precise measurements of occurrence times of discrete events, which is called a time point series. On the other hand, a time series is made of measurements of continuously varying quantities measured at discrete times. For a given period P, a time point series $\{t_i\}$ can be converted into a series of phase angles,

$$\theta_i(P) = 2\pi(t_i/P - m_i) = 2\pi(\nu t_i - m_i), \tag{2}$$

where m_i is an integer portion of (t_i/P). Therefore, we can use the method of analyzing angular distribution of discrete events to study periodicity.

One of often used methods is the Rayleigh analysis method. In this method, each event is represented as a unit vector, and the sum of these unit vectors

$$\vec{R} = \vec{e}_x \sum_{i=1}^{N} \cos 2\pi\nu t_i + \vec{e}_y \sum_{i=1}^{N} \sin 2\pi\nu t_i \tag{3}$$

is considered. The square of this vector divided by N, the number of total events, is defined as the Rayleigh power:

$$z(\nu) = \frac{1}{N}\left[\left(\sum_{i=1}^{N} \cos 2\pi\nu t_i\right)^2 + \left(\sum_{i=1}^{N} \sin 2\pi\nu t_i\right)^2\right]. \tag{4}$$

If occurrence times of events are statistically independent from each other, the Rayleigh power is properly normalized. In other words, the probability for the power at a given frequency to be equal to or greater than z_0 by chance is $\exp(-z_0)$.

However, occurrence times of flares from the same active regions are not independent, but they are separated mostly by less than a week and at most by two weeks. Therefore, for periods much longer than a week, flares from the same active region have similar values of phase angles. In order to overcome this problem, I have developed a method of normalizing the Rayleigh power (Bai 2003). In this method, a cluster of major flares from an individual active region is regarded as a statistically independent unit. Let $\vec{R}_j$ represent the vector sum of individual vectors representing individual flares from the same active region with region index j,

$$\vec{R}_j(\nu) = \vec{e}_x \sum_{k=1}^{n_j} \cos 2\pi\nu t_{jk} + \vec{e}_y \sum_{k=1}^{n_j} \sin 2\pi\nu t_{jk} \tag{5}$$

where n_j is the number of major flares from the active region with index j, and t_{jk} is the occurrence time of the kth flare from this active region.

If we take the above vector sum as a statistically independent unit, studying periodicities of flare occurrences is analogous to *a random-walk problem with varying step sizes,* where $\vec{R}_j$ is the jth step of the random walker. The vector sum

$$\vec{R}(\nu) = \sum_{j=1}^{n} \vec{R}_j(\nu), \tag{6}$$

indicates the displacement of the random walker from the origin after n steps. The probability of finding the random walker at a distance equal to or greater than r_0 is given by

$$Pr(r \geq r_0) = \exp\left\{-\frac{1}{n}(r_0/S)^2\right\}, \tag{7}$$

where S is the r.m.s. step size given by

$$S = \sqrt{\sum_{j=1}^{n} R_j^2/n}. \tag{8}$$

Therefore, if we define the normalized Rayleigh power as

$$z_{nor}(\nu) = \frac{1}{n}(R/S)^2 = \frac{R^2}{\sum_{j=1}^{n} R_j^2} \tag{9}$$

it is properly normalized. Expressing explicitly as a function of vector components representing individual events, we obtain

$$z_{nor}(\nu) = \frac{\left[\sum_{j=1}^{n}\sum_{k=1}^{n_j}\cos 2\pi\nu t_{jk}\right]^2 + \left[\sum_{j=1}^{n}\sum_{k=1}^{n_j}\sin 2\pi\nu t_{jk}\right]^2}{\sum_{j=1}^{n}\left\{\left[\sum_{k=1}^{n_j}\cos 2\pi\nu t_{jk}\right]^2 + \left[\sum_{k=1}^{n_j}\sin 2\pi\nu t_{jk}\right]^2\right\}}. \tag{10}$$

In this paper, the power spectrum calculated with this equation is called a normalized Rayleigh spectrum or simply a power spectrum.

Comparing equation (9) with equation (4), we find the normalization factor is given by

$$F_{nor} = \frac{N}{\sum_{j=1}^{n} R_j^2}. \tag{11}$$

This is a function of frequency because the vectors $\vec{R}_j$ depend on frequency. For periods much longer than a week (one week is a typical duration during which a prolific active region stays prolific), the phase angles of the flares from the same active region are similar to each other. Therefore, in this case, $R_j \simeq n_j$. However, as the period becomes shorter, differences between the phase angles of the flares from the same active region become larger, and R_j becomes smaller than n_j.

Bai (1992a,b) normalized the Rayleigh spectrum by dividing by a constant factor, after empirically inspecting the distribution of power. However, such a normalization will be erroneous unless the periodicity under consideration is near the middle of the frequency range chosen as a search window.

2.4. The maximum likelihood method

In the maximum likelihood method, one assumes a phase angle distribution function, $f(\theta; p_1, p_2)$, where p_1 and p_2 are free parameters defining f. For each event, the probability for finding an event at a phase angle θ_i is $f(\theta_i; p_1, p_2)$. The joint probability for finding N events with $\{\theta_1, \theta_2, \theta_3, \cdots, \theta_N\}$ is given by

$$M(\nu; p_1, p_2) = \prod_{i=1}^{N} f(\theta_i; p_1, p_2). \tag{12}$$

Taking logarithms of the both sides, we obtain the logarithmic likelihood

$$m(\nu; p_1, p_2) = \ln M(\nu; p_1, p_2) = \sum_{i=1}^{N} \ln f(\theta_i; p_1, p_2). \tag{13}$$

In the maximum likelihood method, for each frequency the parameters p_1 and p_2 are adjusted to maximize the likelihood function. Thus, we can define the "maximum likelihood spectrum" as

$$m_{max}(\nu) = \left[\sum_{i=1}^{N} \ln f(\theta_i(\nu); p_1, p_2) \right]_{max}. \tag{14}$$

Bai (1992b) compared the Rayleigh analysis with the maximum likelihood method using a sinusoidal function as a phase angle distribution function

$$f(\theta) = [1 + A\cos(\theta - \theta_0)], \tag{15}$$

where A and θ_0 are two free parameters. He found that the maximum likelihood spectrum is numerically almost the same as the Rayleigh spectrum for large values of N. It is also found that the Rayleigh power z and the amplitude A_m that maximizes the likelihood is related by

$$z = 0.25NA_m^2. \tag{16}$$

Therefore, for the same amplitude of modulation, the power is proportional to the number of events. By combining equations (4) and (16), we obtain the relation

$$A_m = 2R/N. \tag{17}$$

In the maximum likelihood method, for each frequency we search for the values of A and θ_0 that maximize the likelihood, but in the Rayleigh analysis method, we can calculate these values directly by using equations (3) and (17). (The angle of $\vec{R}$ is θ_0.) Therefore, Rayleigh analysis requires much less calculations than the maximum likelihood method for finding a periodicity from a time point series. The Rayleigh analysis was used for periodicity analysis of energetic-electron events detected in interplanetary space (Dröge et al. 1990) and solar energetic proton events (Bai & Cliver 1990).

An elegant way of normalizing the maximum likelihood spectrum has not been proposed, which takes flare clustering in active regions into consideration. However, we may use the normalization factor given by equation (11) because the Rayleigh power and the logarithmic maximum likelihood are numerically identical when a sinusoidal function is used as a trial distribution function (Bai 1992b). Then, the normalized maximum likelihood spectrum is defined by

$$m_{nor}(\nu) = \frac{N}{\sum_{j=1}^{n} R_j^2} \left[\sum_{i=1}^{N} \ln f(\theta_i; p_1, p_2) \right]_{max}. \tag{18}$$

The main advantage of the maximum likelihood method is the flexibility in choosing the distribution function $f(\theta; p_1, p_2)$, which is utilized in this paper.

In order to check whether the normalized likelihood spectrum defined above is properly normalized, I calculated powers for 126 frequencies $f_i = (3i + 20)$ nHz, for $i = 0, \cdots, 125$, using major flare occurrence times of cycle 21 as the input data and equation (21) as a distribution function. The distribution of powers is plotted in Figure 1. The fact that the straight line $y = 126\exp(-x)$ gives an excellent fit to the data indicates that the normalization is very good.

After calculating a power spectrum, one has to evaluate the probability that a peak (with a normalized power z_0) in the spectrum is due to chance. According to Scargle (1982), the false alarm probability is given by

$$FAP = 1 - [1 - \exp(-z_0)]^m \tag{19}$$

where m is the number of independent frequencies in the search window from frequency f_1 to f_2. It is calculated by

$$m = \frac{f_2 - f_1}{f_{ind}} = (f_2 - f_1)T \tag{20}$$

where T is the time interval for the data, and f_{ind} is the independent frequency spacing.

3. Analysis Results

3.1. Result for cycle 23

Cycle 23 is in the declining phase, and enough time has passed since its beginning for analysis of flare periodicities. Figure 2 shows the occurrence rate of major flares (GOES class $\geq$ M1.0) as a function of time, which is smoothed with a 27-d moving window. Five epochs of high activity indicated by numbers 1, 2, 3, 4, and 5 seem to be evenly spaced.

Figure 3 shows power spectra for two time intervals of cycle 23. Figure 3a shows the power spectrum for the interval from the beginning of cycle 23 to 2002 October 10. A peak at 45 nHz (257.2 d) has a power of 5.81. (A frequency f and its corresponding period P are numerically related by $f = 11,574/P$ when nHz and d are units.) However, this periodicity is not statistically significant.

Figure 3b is the power spectrum for the interval from 1999 September 9 to 2001 June 5, during which the five epochs of high activity identified in Figure 2 occurred. Flares occurring near minimum phases of a given periodicity decrease the Rayleigh power for this periodicity while flares occurring near maximum phases increase it. Therefore, in order to fairly assess the strength of a periodicity, one should choose the time interval for spectral analysis so that it start at a minimum phase of the periodicity under investigation and end at another minimum phase. In the lower panel, we find peaks at 129 d and its harmonic period. The FAP for the 129-d periodicity is 5.6%. The amplitude of modulation of the best-fit sinusoidal function is found to be 0.73. If I analyze flares selected with a higher threshold, M3.0, the amplitude of modulation increases slightly to 0.76, but the peak power decreases to 4.06. The decrease of power is due to a decrease of the number of active regions producing the selected flares.

From flares with GOES classes $\geq$M3.0, I detected a 33.5-d periodicity. Figure 4 shows spectra for the interval from 1999 October 4 to 2001 April 21, which corresponds to 17 cycles of the 33.5 d period. In the spectrum for flares above M3.0, the 33.5-d peak has a power of 6.06, but in the spectrum for flares above M1.0, this peak is negligible. The amplitude of

modulation for flares above the threshold M3.0 is 0.88, but it is only 0.47 for flares above the threshold M1.0. We can infer that this periodicity is more effective for energetic flares than for less energetic flares. The FAP for the peak in Figure 4a is 4.6%.

The 62.6-d and 125.8-d peaks in Figure 4b are bigger than the corresponding peaks in Figure 3b. This is because the time interval for Figure 4b does not include some flares produced near the minimum phases of these periodicities. Therefore, these peaks in Figure 4b overestimate the strengths of these periodicities.

Figure 5 shows phase diagrams for the two periodicities mentioned above. The phase diagram for 33.5-d periodicity is well fit by a sinusoidal function. On the other hand, the phase diagram for the 129-d periodicity is not well represented even by the best-fit sinusoidal function. From this we can infer the following. The 129-d peak in Figure 3b is not large in spite of a large modulation of the phase diagram (Fig. 5a) because the Rayleigh spectrum is equivalent to a maximum likelihood spectrum using a sinusoidal function as a distribution function.

Therefore, let us try an alternative distribution function to be substituted in equation (18), which is a step function given by

$$f(x; x_0, h) = \begin{cases} 1+h & : \quad (x_0 - 0.1) < x < (x_0 + 0.1) \\ 1 - 0.25h & : \quad otherwise \end{cases} \tag{21}$$

where the range of phase $x = \theta/2\pi$ is from 0 to 1, the range of h is 0 to 4, and $x_0 = \theta_0/2\pi$. This expression is for the case when x_0 is between 0.1 and 0.9. For cases $x_0 < 0.1$ and $x_0 > 0.9$, the same form of step function is used but the mathematical expressions become more complicated. This distribution function represents periodic increases of flare activity, whose duration is two tenth of the period. In comparison, a sinusoidal distribution function represents a periodic gentle modulation of flare activity.

The normalized maximum likelihood spectrum is shown in Figure 6 for the time interval of Figure 3b. Three peaks are prominent. The most prominent peak at 92.5-nHz (125 d) has a peak value of 9.37. The two other prominent peaks are near periods of 0.5 and 2 times 125 d. The FAP for the 125-d peak is only 0.18%.

For the results shown in Figures 1 and 6, the maximum phase, x_0, for equation (21) was directly calculated by using equation (6). If we let it vary freely, its value may be somewhat different from what is obtained from equation (6) for cases where maximum likelihood values are very small. However, for large values of maximum likelihood, the maximum phase, x_0, is the same as what is obtained from equation (6).

3.2. Results for cycles 19–21

Several authors have studied periodicities in flare occurrence for cycles 19–21. However, it is necessary to reanalyze these cycles using the new methods for the following reasons. First, applications of the same methods make it easier to compare statistical significances of periodicities detected in different cycles. Second, we can interpret the 128-d periodicity of cycle 23 by finding its relationship with periodicities detected in previous solar cycles.

Figure 7 shows the normalized Rayleigh spectrum for cycle 19, which shows one prominent peak at f=227 nHz (51.0 d), consistently with Bai (1987). The false alarm probability for this peak is 2.5% when $m = 120$ and $z_0 = 8.48$ are substituted into equation (19).

Autocorrelation functions of time profiles can reveal some aspects of periodicities. In this paper, the following autocorrelation function is used:

$$X(\Delta i) = \prod_{i=1}^{last-\Delta i} f(i)f(i+\Delta i) \tag{22}$$

where $f(i)$ is the 27-d running mean of the daily major flare number for day number i. Figure 8 shows the result for cycle 19, with dotted vertical lines drawn at integral multiples of 51 d and solid vertical lines for every fifth multiple of 51 days. Peaks in the autocorrelation function appear very regularly at every integral multiple of 51-d except for 26, 28, 31, 38. This figure shows that the 51-d period was in operation for more than 40 periods during cycle 19. (For comparison, the current solar cycle is the 28th cycle since the Maunder Minimum.)

Now let us turn to cycle 20. Figure 9 shows the 27-d running mean of the flare occurrence rate of cycle 20. The top panel is for the entire cycle. Time profiles for the intervals indicated by a dashed line and a solid line in Figure 9a are shown in Figures 9b and 9c. Here we can notice periodic modulations with the 84-d period and the 128-d period.

Figure 10 shows normalized Rayleigh spectra for three time intervals of cycle 20. The top panel, which is for the entire cycle, shows two big peaks at f=89 nHz and f=138 nHz. However, the false alarm probability even for the bigger peak is as large as 20%. Figure 10b is for the interval from 1996 February 9 to 1968 March 6, during which 84.5-d periodicity was in operation continuously. The 85-d peak in Figure 10b is not bigger than the 85-d peak in Figure 10a. This means that the power for the 85-d periodicity is not exclusively from the time interval for Figure 10b. Although the 85-d peak is not impressive at all, its amplitude of modulation is found to be as large as 0.95. This is because the power depends not only on the amplitude of modulation but also on the number of events. During the period for which the power spectrum in Figure 10b is calculated, only 34 active regions produced major flares numbering 73.

Figure 10c is for the interval from 1980 August 20 to 1983 June 5. The 129-d peak here, with a value of 6.11, is bigger than the corresponding peak in Figure 9a. It means that this periodicity was in operation mainly during the time interval mentioned in Figure 10c. The amplitude of sinusoidal modulation for the phase diagram of this periodicity is found to be 0.78. The false alarm probability for the 129-d periodicity is 7.3%.

Figure 11 shows normalized Rayleigh spectra for two intervals of cycle 21. Figure 11a is for the entire cycle; Figure 11b, for the interval from 1980 March 19 to 1983 May 6. The false alarm probability for the 152-d peak in Figure 11b is 0.72%, and its amplitude of modulation is 0.83.

Table 1 shows analysis results for flares selected with different selection criteria, for the interval mentioned in Figure 11b. The amplitude of modulation increases as the threshold increases (cf. Bai 1993). The amplitudes greater than 1 are mathematically allowed although unphysical. The peak power, however, does not keep on increasing with increasing threshold because the peak power also depends on the number of active regions involved. The largest peak is obtained from flares with X-ray classes $\geq$M7.0. The normalized peak power for GRS flares is found to be 9.55, while the unnormalized Rayleigh power at 75 nHz is 25.68, which is consistent with the result of Dröge et al. (1990). It is obvious that a simple application of Rayleigh analysis to solar flares leads to a gross overestimation of the statistical significance of a periodicity.

Let us summarize the results for cycles 19–21. During most of the entire cycle 19, the 51-d periodicity was in operation, at least for 40 periods. During cycle 20, two periodicities (84-d and 129-d) were in operation. However, the 84-d periodicity is not statistically very significant. The 153-d periodicity was the only periodicity for cycle 21, even though it operated during a limited time interval of about 8 periods of 153 d.

3.3. Result for cycle 22

Several authors analyzed flare periodicities for cycle 22. By analyzing occurrence times of major flares of 1988 March to 1991 November, Bai (1992a) found a 73-d periodicity, but he emphasized the 77-d periodicity found in the data from 1988 November 18 to 1990 February 23 because this period is 3 times the fundamental period proposed by Bai & Sturrock (1991). Ozguc & Atac (1994) also found a 73-d periodicity by analyzing daily flare indices for the interval from 1986 September through 1991 December. Bai (1994) found a 51-d periodicity from the flare occurrence times from 1991 May 4 to 1992 November 15. Oliver & Ballester (1995) emphasized the lack of the 153-d periodicity in the flare occurrence times of cycle 22.

Considering that different authors applied different methods to different data sets, it seems necessary to reanalyze periodicity for cycle 22 with the new methods. Figure 12 shows power spectra for occurrence times of major flares (≥M.30) for different time intervals of cycle 22. Figure 12a shows the power spectrum for the time interval which was analyzed by Ozguc & Atac (1994). The strongest peak is at 73 d, in agreement with Ozguc & Atac (1994) and Bai (1992a), but it is not statistically significant. In the spectrum obtained by Ozguc & Atac (1994) who analyzed a different data set, however, the 73-d peak was significant. Figure 12b shows the power spectrum for the interval that was analyzed by Bai (1992a), and Figure 12c shows the power spectrum for the interval that was analyzed by Bai (1994). The strongest peaks are at 77 d and 51 d, respectively, in agreement with the earlier results. However, the values of their normalized powers are not large enough to make them statistically significant. Notice that the normalized power for the 51-d peak in Figure 12c is smaller than the normalized power of the same peak in Figure 7 of Bai (1994). This is because Bai (1994) used a constant normalization factor for the whole frequency range (0–900 nHz), whereas the proper normalization factor is a function of frequency as discussed in the previous section.

The amplitude of modulation (cf. eq. 17) corresponding to the three peaks in Figure 12 are 0.46, 0.69, and 0.63, respectively. The amplitudes of modulation for the latter two cases are moderately large, but their powers are not large. This is because these periodicities did not last long and the number of active regions producing major flares during the intervals were not large. I have also analyzed flares selected with different thresholds of X-ray classes, but I have not found any statistically significant periodicities.

4. Summary and Discussion

Several periodicities have been detected from analyses of cycles 19–23: 51 d from cycle 19; 85 and 129 d from cycle 20; 153 d from cycle 21; 34 and 129 d from cycle 23. The 73-d, 77-d, and 51-d periodicities, which were previously reported to be detected from cycle 22, turn out to be statistically not significant.

Let us discuss the properties of these periodicities. First, the detection of the 129-d periodicity from cycle 23 lends support to the idea (Bai & Sturrock 1991) that 25.5 d is a fundamental period of the Sun and solar flare activity often exhibits periodicities at its subharmonic periods. Table 2 summarizes all the periodicities detected in the 30–300 d range from analyses of solar flare occurrences. Except for 33.5-d and 85-d periodicities, all the periodicities have periods very close to integral multiples of 25.5 d. Additionally, analyses of daily sunspot areas have detected periodicities at 51 d (Pap et al. 1990) and 78 d (Bai &

Sturrock 1991).

Second, except for the 34-d periodicity, all the periodicities are visually recognizable in time profiles of flare rates smoothed with a 27-d moving window. Third, periodicities with periods of integral multiples of 25.5 d operated mainly during maximum phases of solar cycles only for short time intervals. Typically, the numbers of periodic episodes repeated are from 5 to 9. Exceptionally, the 51-d periodicity detected in cycle 19 lasted for more than 40 cycles. Fourth, in general, amplitudes of modulation tend to increase with increasing peak X-ray fluxes. The 153-d periodicity of cycle 21 shows this trend (cf. Table 1). Such a trend is shown most strongly in the 34-d periodicity, but it is weak for the 129-d periodicity of cycle 23. This trend has not been analyzed for periodicities detected from cycles 19 and 20.

As for a mechanism for the fundamental period, Bai & Sturrock (1993) proposed an obliquely rotating structure (or wave pattern). This was made on the basis that the longitude distribution of major flares of cycles 19–22 (1955 January 1 to 1990 January 31) exhibits a strong bimodal distribution in a coordinate system rotating with a period of 25.5 d about an axis tilted by 40° with respect to the solar rotation axis. The direction of the tilt is toward the Earth's position on December 4 in its annual orbit.

Stimulated by this paper, Goode & Thompson (1992) and Gough & Kosovichev (1992) investigated the possibility that the inner core of the Sun rotate solidly about an axis tilted by 40°, using helioseismological data. The two papers both concluded that the radius of such an obliquely rotating core should be less than 30% of the solar radius. It is, however, difficult to imagine that such a small obliquely rotating core can influence flare activity occurring on the surface.

Recently Bai (2003) studied longitude distributions of major flares in a coordinate systems rotating about the solar axis, using the rotation period as a free parameter. One of the hot spot systems is a double hot spot system rotating with a synodic period of 27.41 d. This hot spot system operated in the northern hemisphere during cycles 19 through 21. The synodic period of 27.41 d corresponds to the sidereal period of 25.50 d. Therefore, it is clear that this hot spot system and a strong bimodal distribution in the coordinate system obliquely rotating with a sidereal period of 25.50 d are two manifestations of the same phenomenon. It is possible that the double hot spot system in the northern hemisphere gave rise to a strong signal for an obliquely rotating structure by chance. The reverse is also a possibility.

In conclusion, the idea that 25.5 d is a fundamental period of the Sun is well supported by data. However, its clock mechanism is still unknown.

This research was supported by NSF grant ATM-0102184.

REFERENCES

Bai, T. 1987, ApJ, 318, L85

Bai, T. 1992a, ApJ, 388, L69

Bai, T. 1992b, ApJ, 397, 584

Bai, T. 1993, ApJ, 404, 805

Bai, T. 1994, Sol. Phys., 150, 385

Bai, T. 2003, ApJ, 585, 1114

Bai, T., & Cliver, E. W. 1990, ApJ, 363, 299

Bai, T., & Sturrock, P. A. 1987, Nature, 327, 601

Bai, T., & Sturrock, P. A. 1991, Nature, 350, 141

Bai, T., & Sturrock, P. A. 1993, ApJ, 409, 476

Ballester, J. L., Oliver, R., & Baudin, F. 1999, ApJ, 522, L153

Bogart, R. S., & Bai, T. 1985, ApJ, 299, L51

Carbonell, M., & Ballester, J. L. 1990, A&A, 238, 377

Carbonell, M., & Ballester, J. L. 1992, A&A, 255, 350

Dennis, B. R. 1985, Sol. Phys., 100, 465

Dodson, H. W., & Hedeman, E. R. 1971, An Experimental, Comprehensive Flare Indices and Its Derivation for "Major" Flares, 1955-1969, World Data Center for Solar-Terrestrial Physics Report UAG-14, Boulder: NOAA

Dodson, H. W., & Hedeman, E. R. 1975, Experimental Comprehensive Solar Flare Indices for Certain Flares, 1970-1974, World Data Center for Solar-Terrestrial Physics Report UAG-52, Boulder: NOAA

Dodson, H. W., & Hedeman, E. R. 1981, Experimental Comprehensive Solar Flare Indices for "Major" and Certain Lesser Flares, 1975-1979,World Data Center for Solar-Terrestrial Physics Report UAG-80, Boulder: NOAA

Dröge, W. Gibbs, K., Grunsfeld, J. M., Meyer, P., & Newport, B. J. 1990, ApJS, 73, 279

Gabriel, S., Evans, R., & Feynman, J. 1990, Sol. Phys., 128, 415

Goode, P., & Thompson, M. 1992 ApJ, 395, 307

Gough, D. O., & Kosovichev, A. G. 1992, in IAU Colloq. 137, Inside the Stars, San Francisco: ASP

Ichimoto, K., Kubota, J., Suzuki, M., Tohmura, I., & Kurokawa, H. 1985, Nature, 316, 422

Kile, J. N., & Cliver, E. W. 1991, ApJ, 370, 442

Krivova, N. A., & Solanki, S. K. 2002, A&A, 394, 701

Landscheidt, T. 1986, Sol. Phys., 107, 195

Lean, J. L. 1990, ApJ, 363, 718

Lean, J. L., & Brueckner, G. E. 1989, ApJ, 337, 568

Mardia, K. V. 1972, Statistics of Directional Data, New York: Academic Press

Oliver, R., & Ballester, J. L. 1995, Sol. Phys., 156, 145

Oliver, R., Ballester, J. L., & Baudin, F. 1998, Nature, 394, 552

Ozguc, A., & Atac, T. 1989, Sol. Phys., 123, 357

Ozguc, A., & Atac, T. 1994, Sol. Phys., 150, 339

Pap, J., Tobsika, W. K., & Bouwer, S. D. 1990, Sol. Phys., 129, 165

Rieger, E., Share, G. H., Forrest, D. J., Kanbach, G., Reppin, C., & Chupp, E. L. 1984, Nature, 312, 623

Scargle, J. D. 1982, ApJ, 263, 835

Verma, V. K., & Joshi, G. C. 1987, Sol. Phys., 114, 415

Table 1: 153-day Periodicity of Cycle 21 (1980 Mar 9 – 1983 Jul 16).

Threshold	Peak freq.	Peak power	Amplitude	Event #	A.R. #	FAP(%)
M1.0	75 nHz	8.51	0.68	1354	260	0.80
M3.0	76 nHz	8.74	0.81	408	129	0.64
M5.0	75 nHz	9.27	0.90	222	91	0.38
M7.0	75 nHz	11.11	1.01	159	73	0.06
X1.0	75 nHz	9.16	1.06	98	50	0.42
GRS[a]	74 nHz	9.55	0.92	126	72	0.28

[a]Detection by the gamma ray spectrometer aboard SMM.

Table 2: Periodicities Detected from Solar Flare Occurrence.

Period (d)	Epoch	Flare selection criterion	Reference
33.5	Cycle 23	GOES class ≥M3.0	This paper
51	Cycle 19	CFI≥6	Bai 1987
51	Cycle 19	10 cm radio wave ≥200 sfu	Kile & Cliver 1991
78	Cycle 20	Microwave ≥10 sfu	Bogart & Bai 1985
84	1970–1982	GOES class ≥X1.0	Landscheidt 1987
84	Cycle 20	CFI≥7	Bai & Sturrock 1991
129	Cycle 20	CFI≥7	Bai & Sturrock 1991
129	Cycle 20	CFI≥6	Kile & Cliver 1991
129	Cycle 23	GOES class ≥M1.0	This paper
153	1980–1983	γ rays ≥270 keV	Rieger et al. 1984
153	1980–1983	GOES class ≥M2.5	Rieger et al. 1984
153	Cycle 21	Hα emission	Ichimoto et al. 1985
153	Cycle 20	Hα emission	Ichimoto et al. 1985
153	Cycle 21	Hard X ray detection by SMM	Dennis 1985
153	Cycle 21	Solar energetic protons	Bai & Cliver 1990
153	Cycles 19 & 20	Solar energetic protons	Bai & Cliver 1990
153	Cycle 21	Solar energetic protons	Gabriel et al. 1990
153	Cycle 21	Solar energetic electrons	Dröge et al. 1990
153	Cycle 21	10 cm radio wave ≥200 sfu	Kile & Cliver 1991

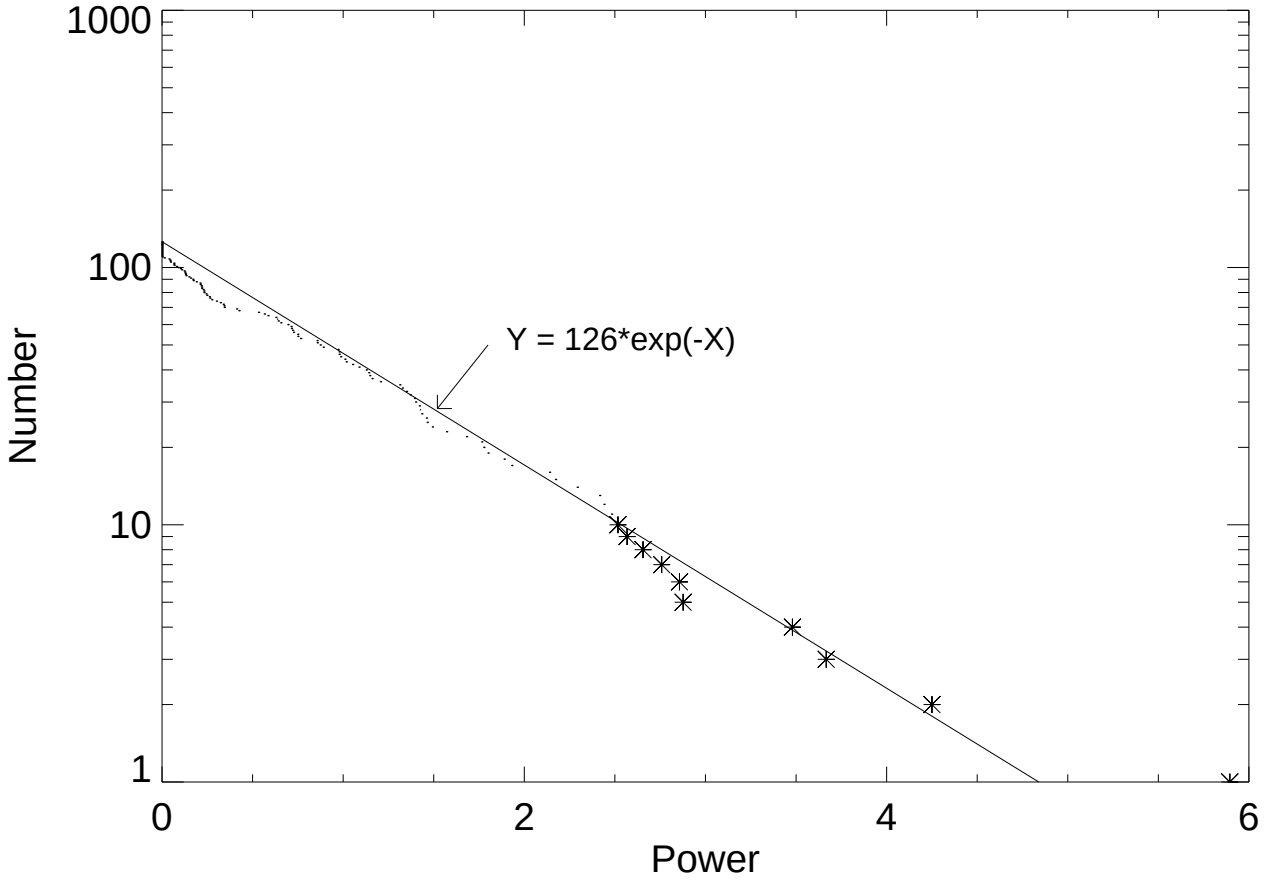

Fig. 1.— Distribution of Powers. The number of cases where powers are equal to or greater than a certain value is plotted as a function of power. Data points are shown by dots, except the last 10 points. Such a distribution is usually well fit by an exponential function $y = N \exp(-x/a)$, where N is the total number of frequencies and a is a normalization constant. The normalization of power is good when $a = 1$, as here.

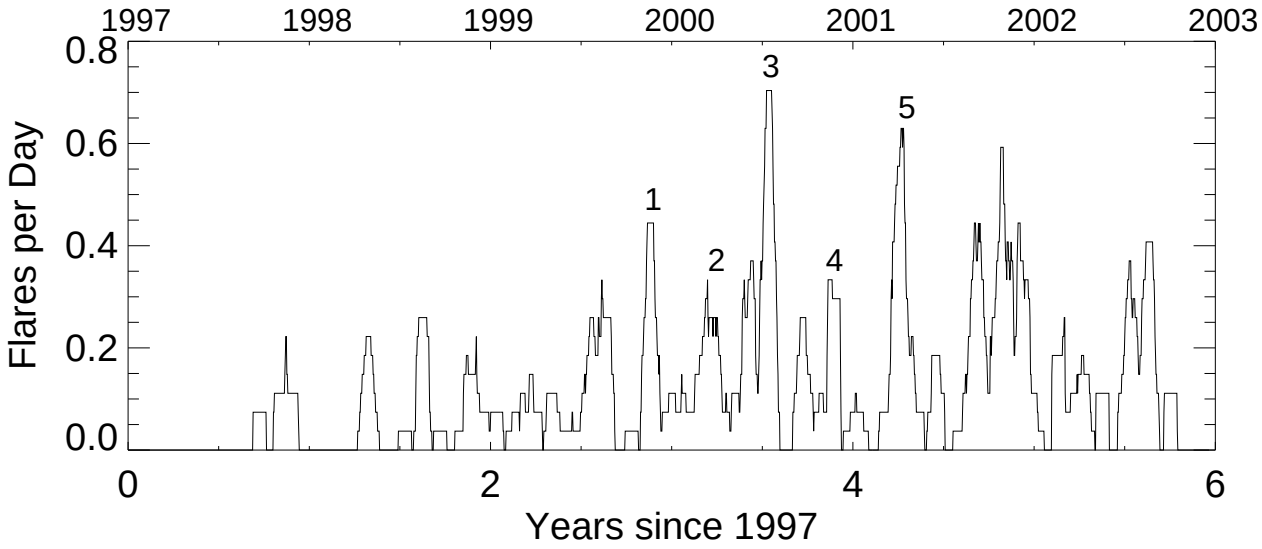

Fig. 2.— Daily number of major flares ($\geq$ M1.0) of cycle 23, smoothed with a 27-*d* moving window. Five epochs of high flare activity, numbered 1 to 5, seem to be equally spaced.

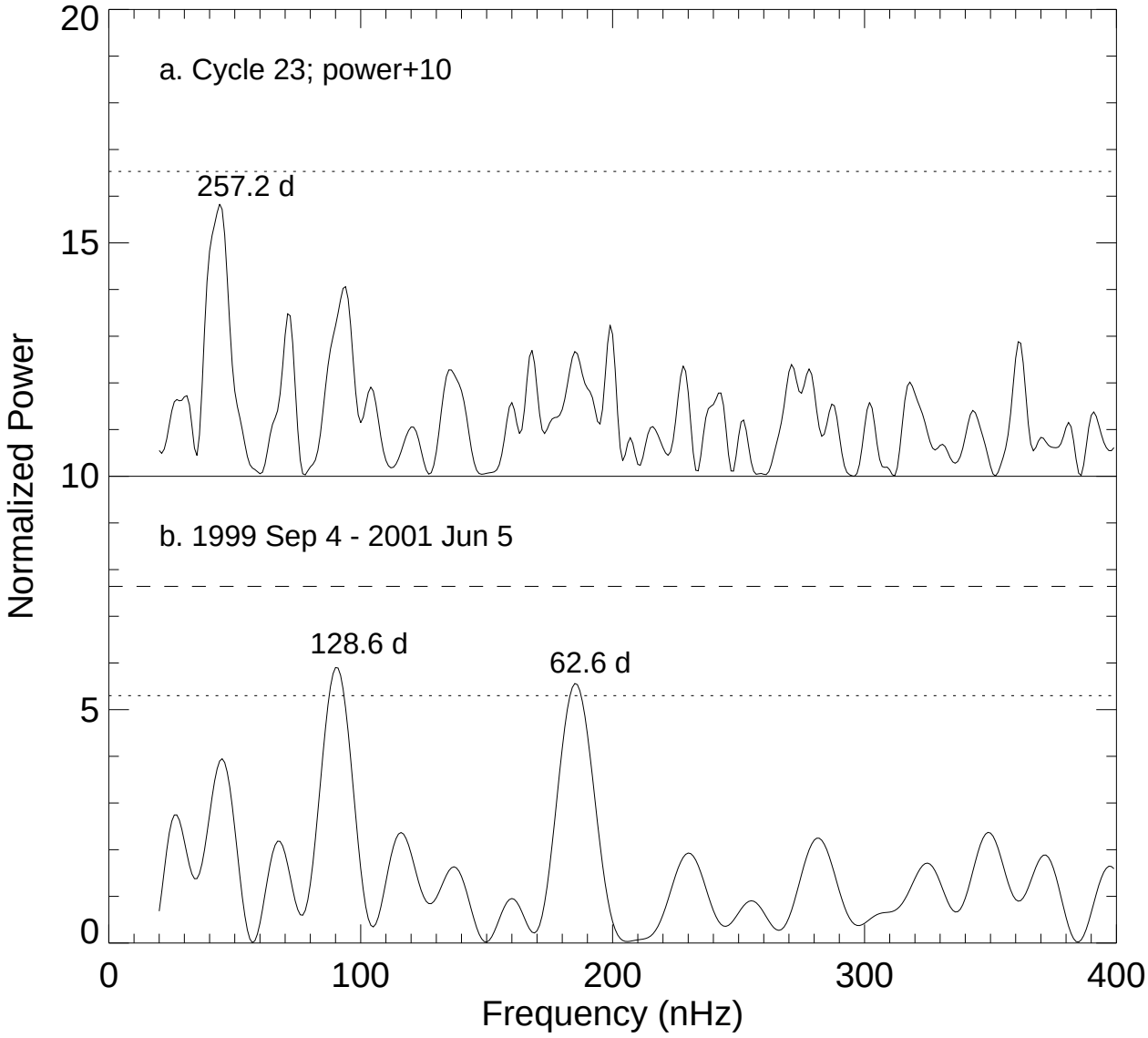

Fig. 3.— Normalized Rayleigh power spectra. The top spectrum is for the interval from the beginning of cycle 23 to 2002 October 15, and the bottom, for a shorter interval specified in the figure. Horizontal dotted lines indicate the FAP level of 10%, and the dashed line in the lower panel is the FAP level of 1%.

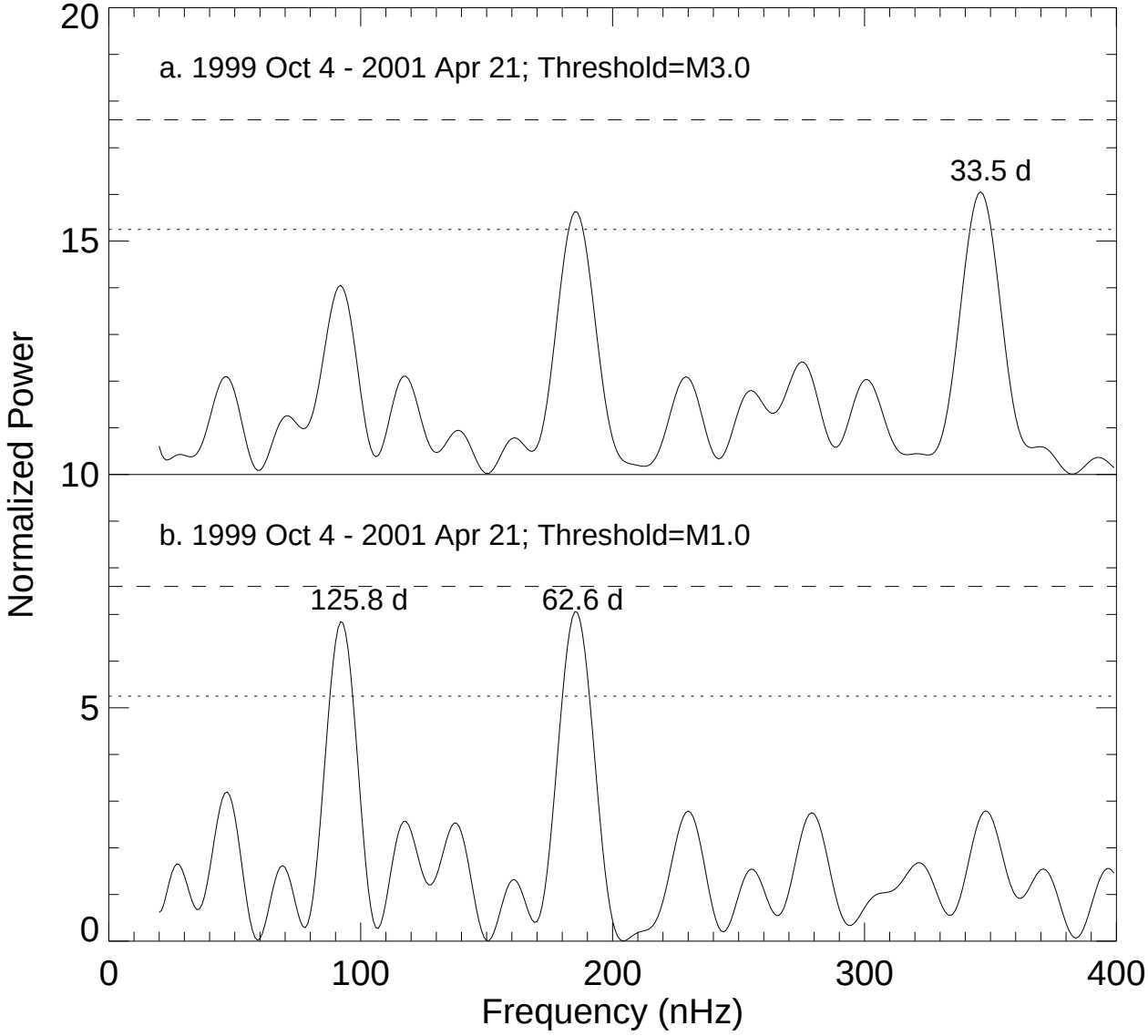

Fig. 4.— Spectra for flares selected with two different thresholds for the same time interval, during which the 33.5-d periodicity was in operation. The dashed and dotted horizontal lines in each panel show the 1% and 10% FAP levels, respectively.

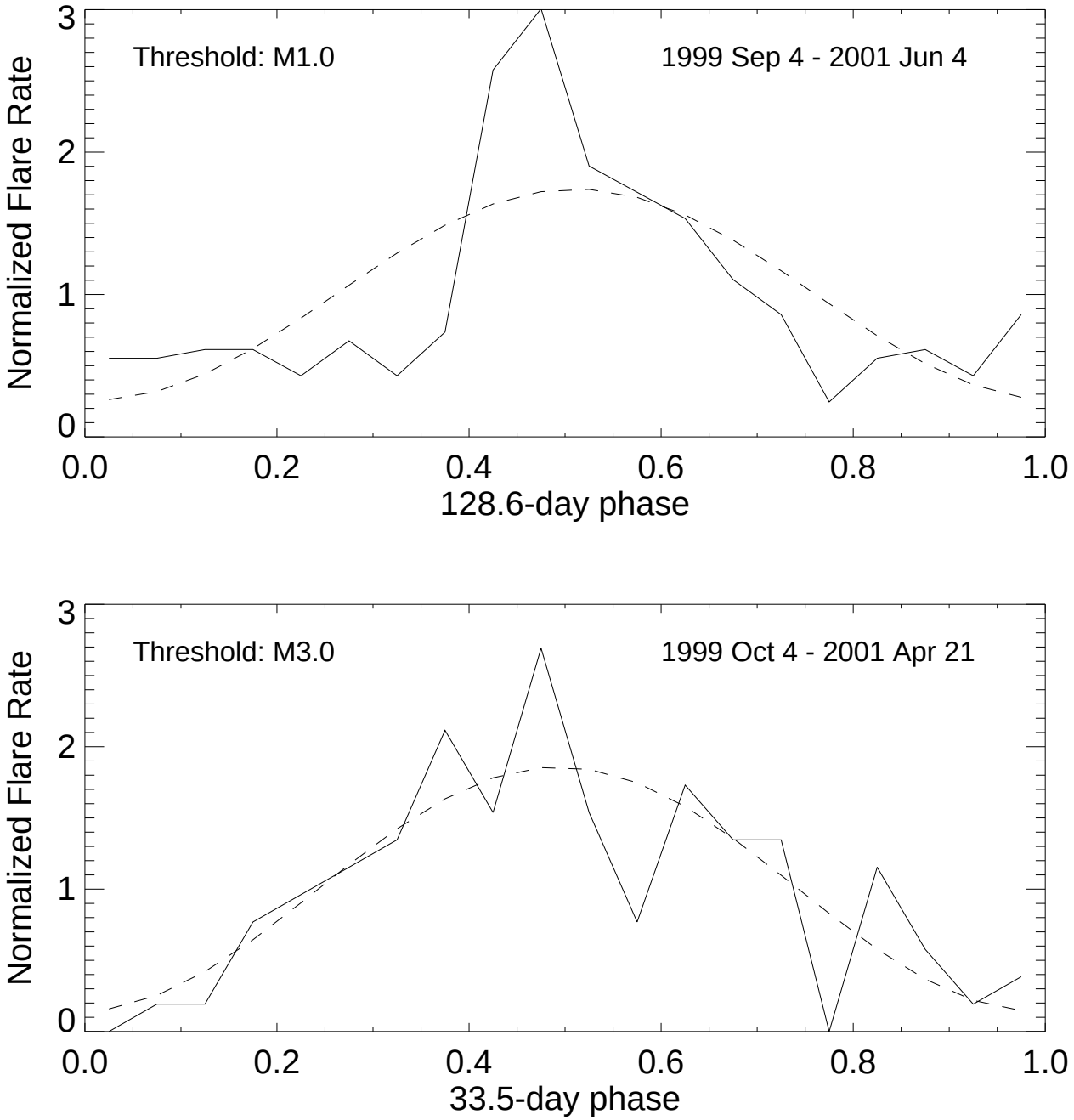

Fig. 5.— Phase diagrams for the 128.6-d and 33.5-d periodicities. The dotted line in the upper panel is the best-fit sinusoidal function, $y = 1 + 0.74 \cos 2\pi(x - 0.511)$. The dotted line in the lower panel is $y = 1 + 0.86 \cos 2\pi(x - 0.493)$. The total number of flares for Fig. 5a is 326, and that for Fig. 5b is 104.

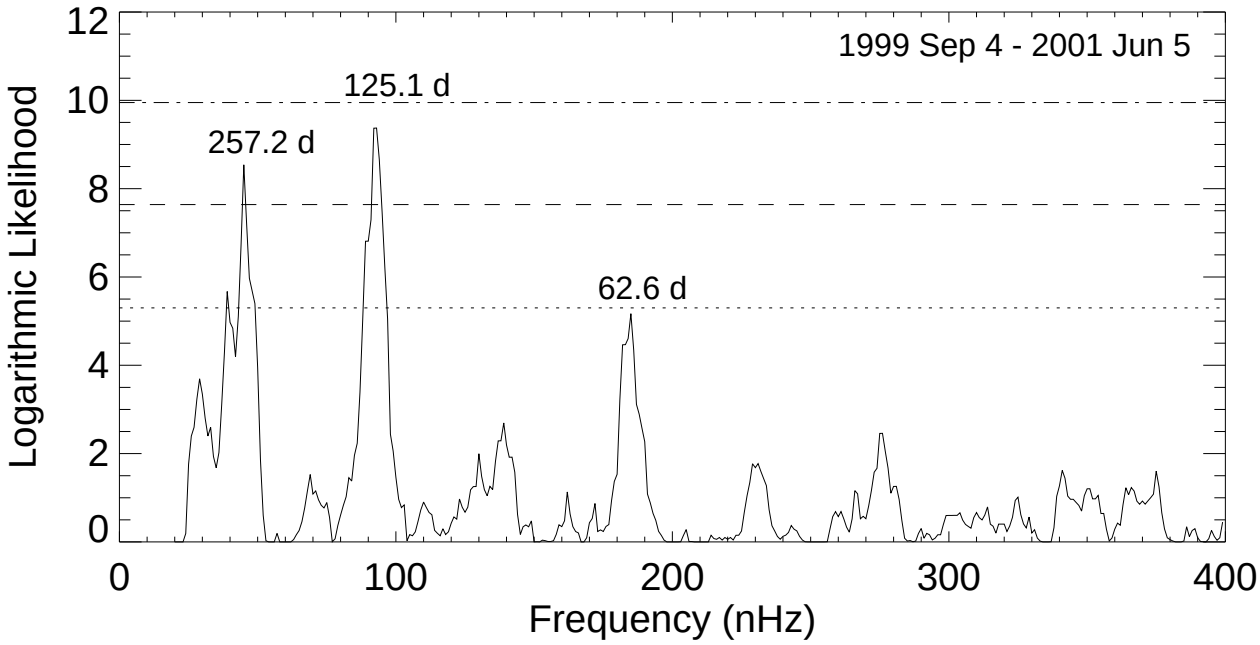

Fig. 6.— Normalized maximum likelihood spectrum. Three prominent peaks here are much bigger than the corresponding peaks in Fig. 3b. Three horizontal lines indicate FAP levels of 10% (dotted), 1% (dashed), and 0.1% (dash-dotted), respectively.

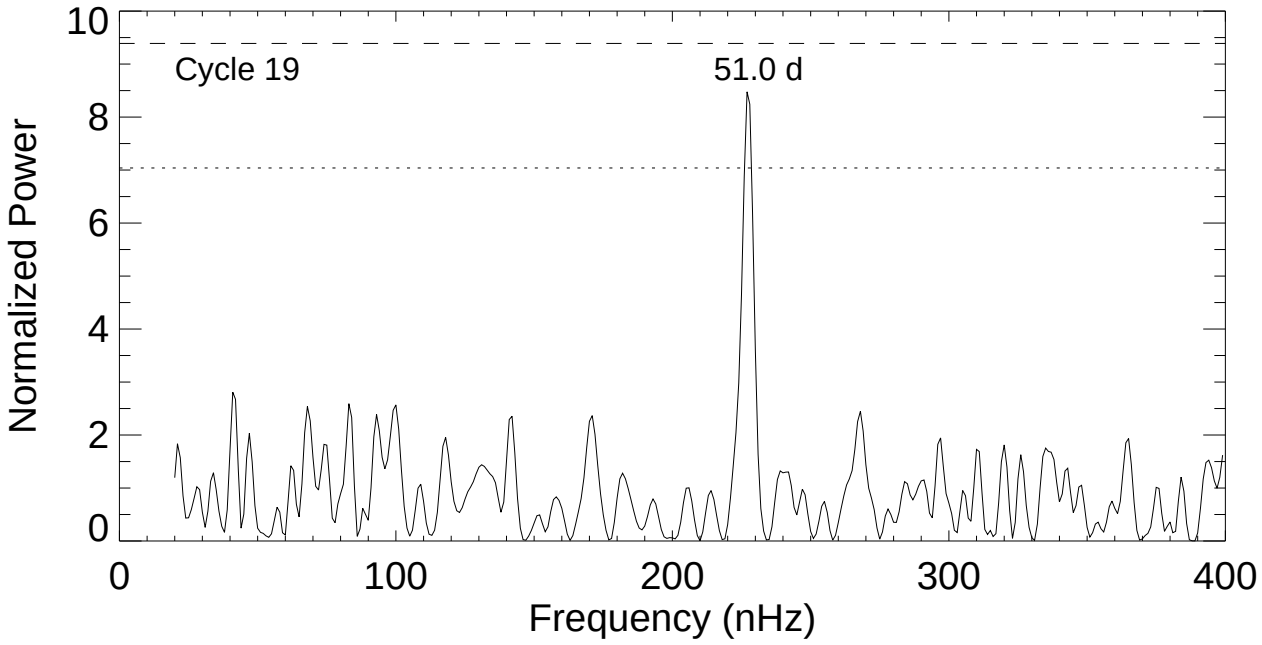

Fig. 7.— Normalized Rayleigh spectrum for cycle 19. FAP levels of 10% and 1% are indicated by two horizontal lines.

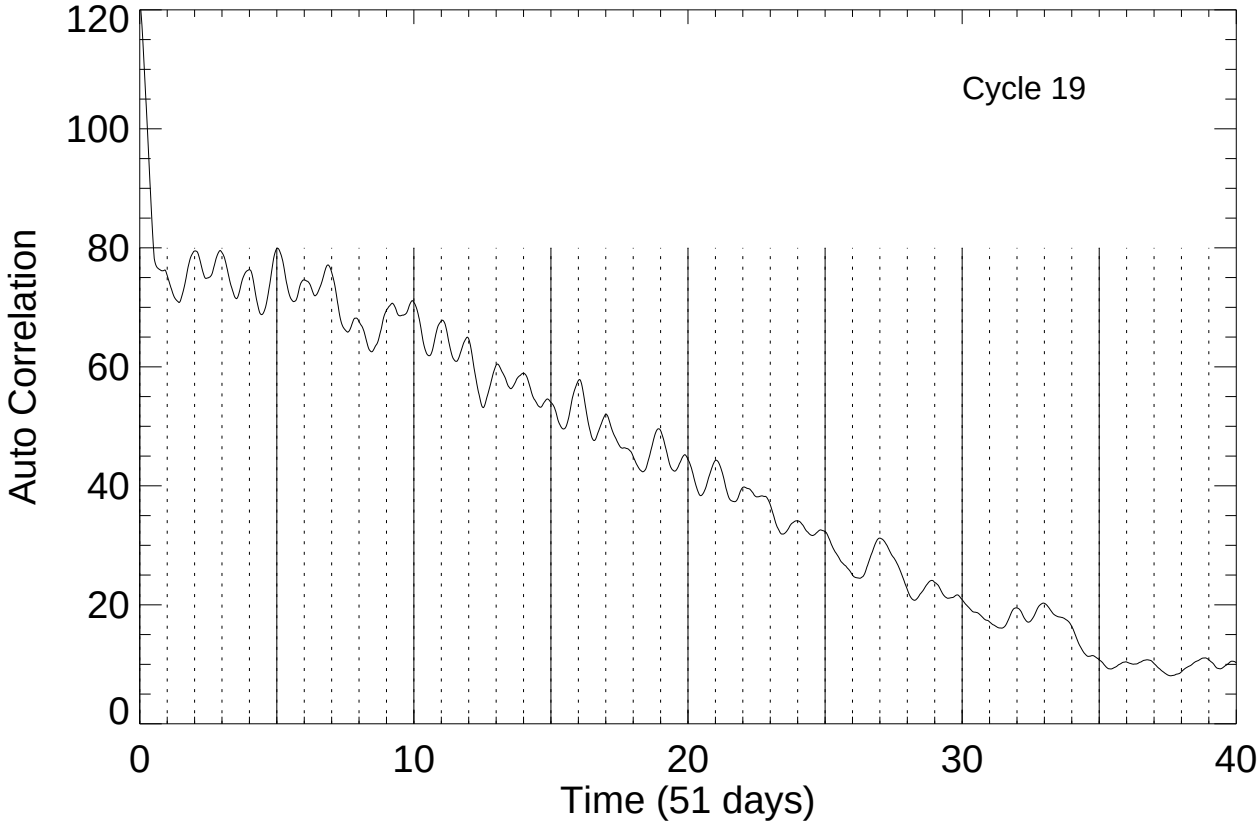

Fig. 8.— Autocorrelation function for the flare rate of cycle 19.

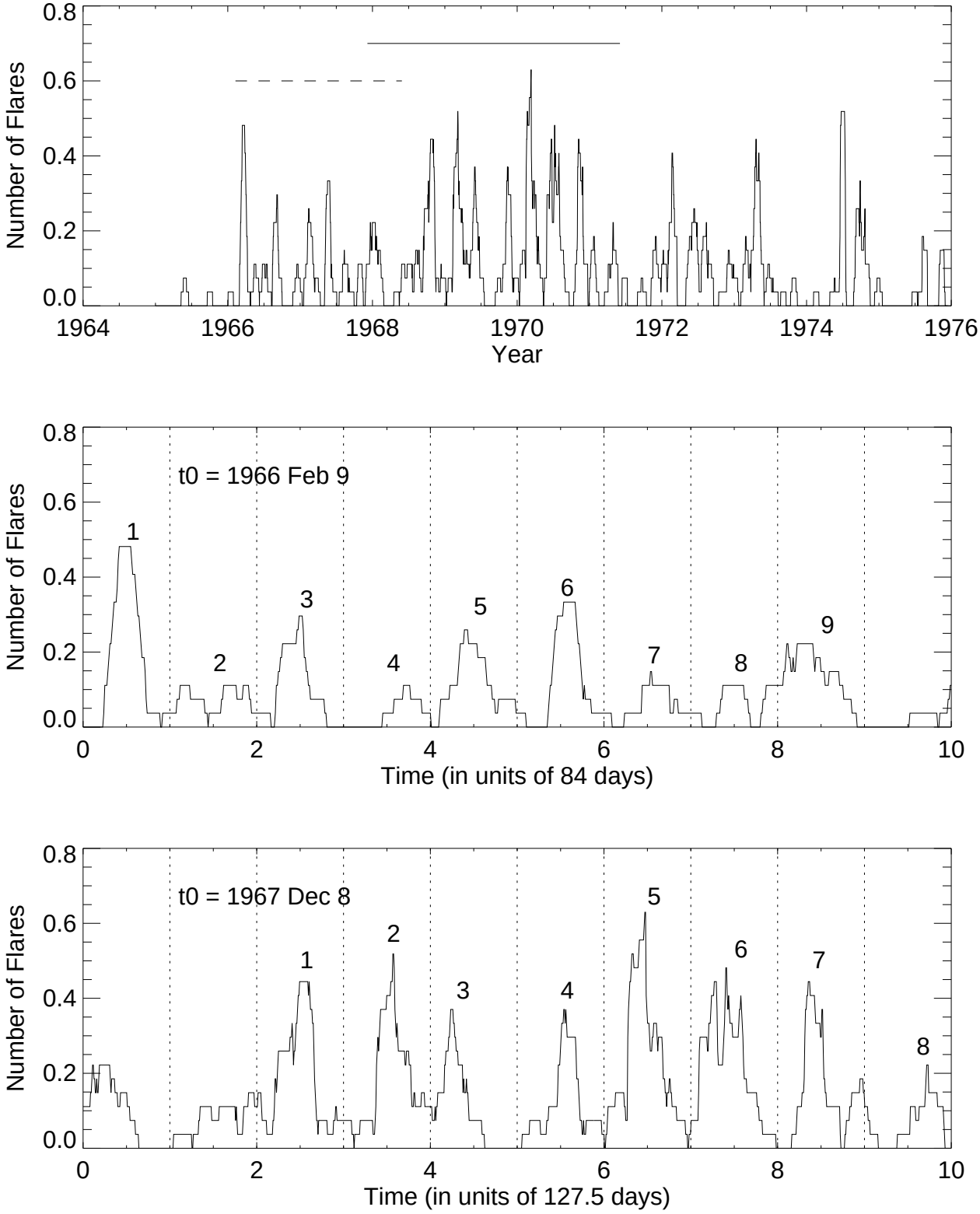

Fig. 9.— Time profiles of the flare rate of cycle 20. The middle panel, which is an expanded plot of the interval indicated by the dashed line in the top panel, shows the 84-d periodicity. The bottom panel, which is an expanded plot of the interval indicated by the solid line in the top panel, shows the 128-d periodicity.

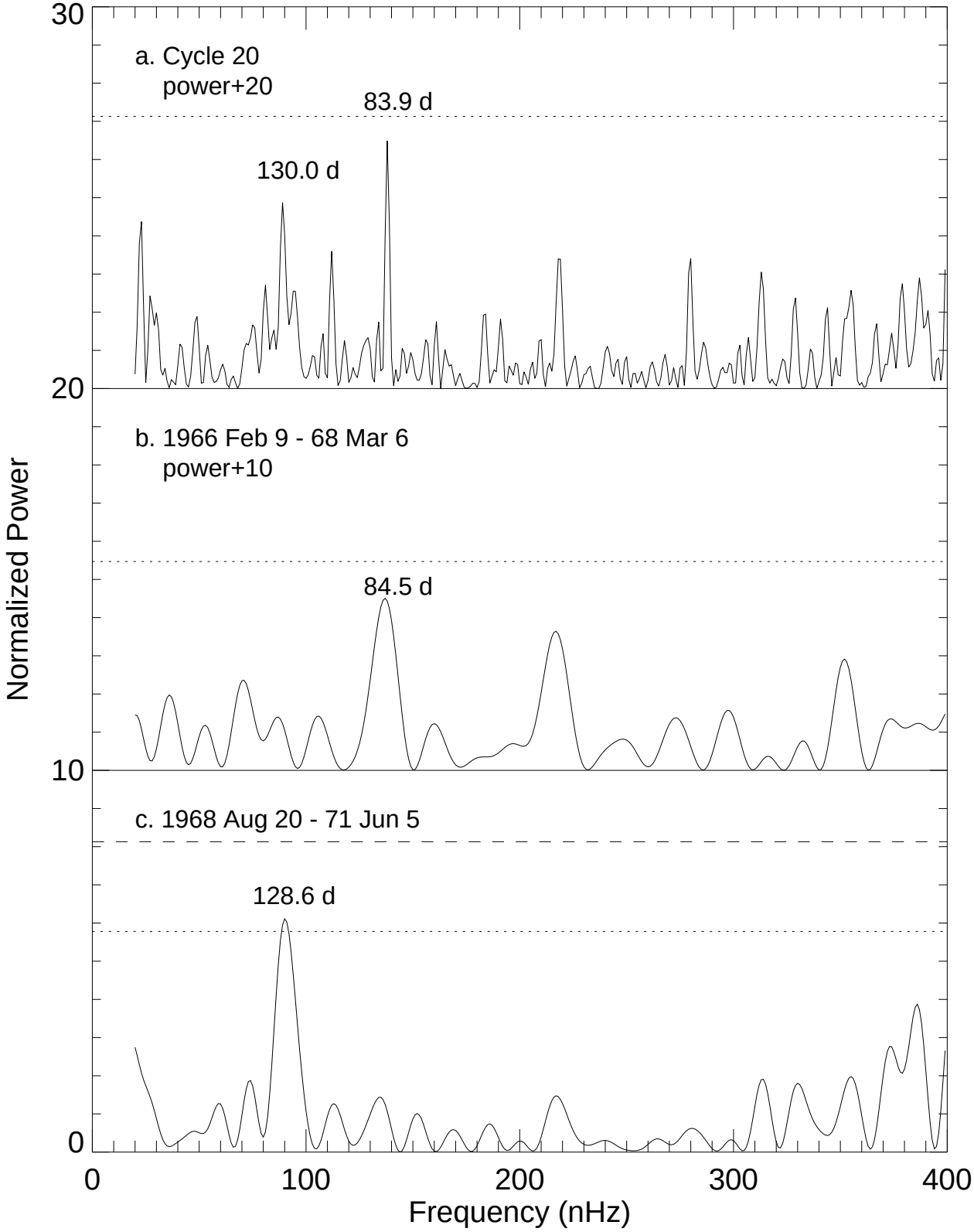

Fig. 10.— Normalized Rayleigh spectra for three intervals of cycle 20. The middle panel is for the 9 cycles of the 84-d periodicity shown in Fig. 9b. The bottom panel is for the 8 cycles of the 129-d periodicity shown in Fig. 9c. Horizontal dotted lines indicate the FAP level of 10%, and the dashed line in the bottom panel indicates the FAP level of 1%.

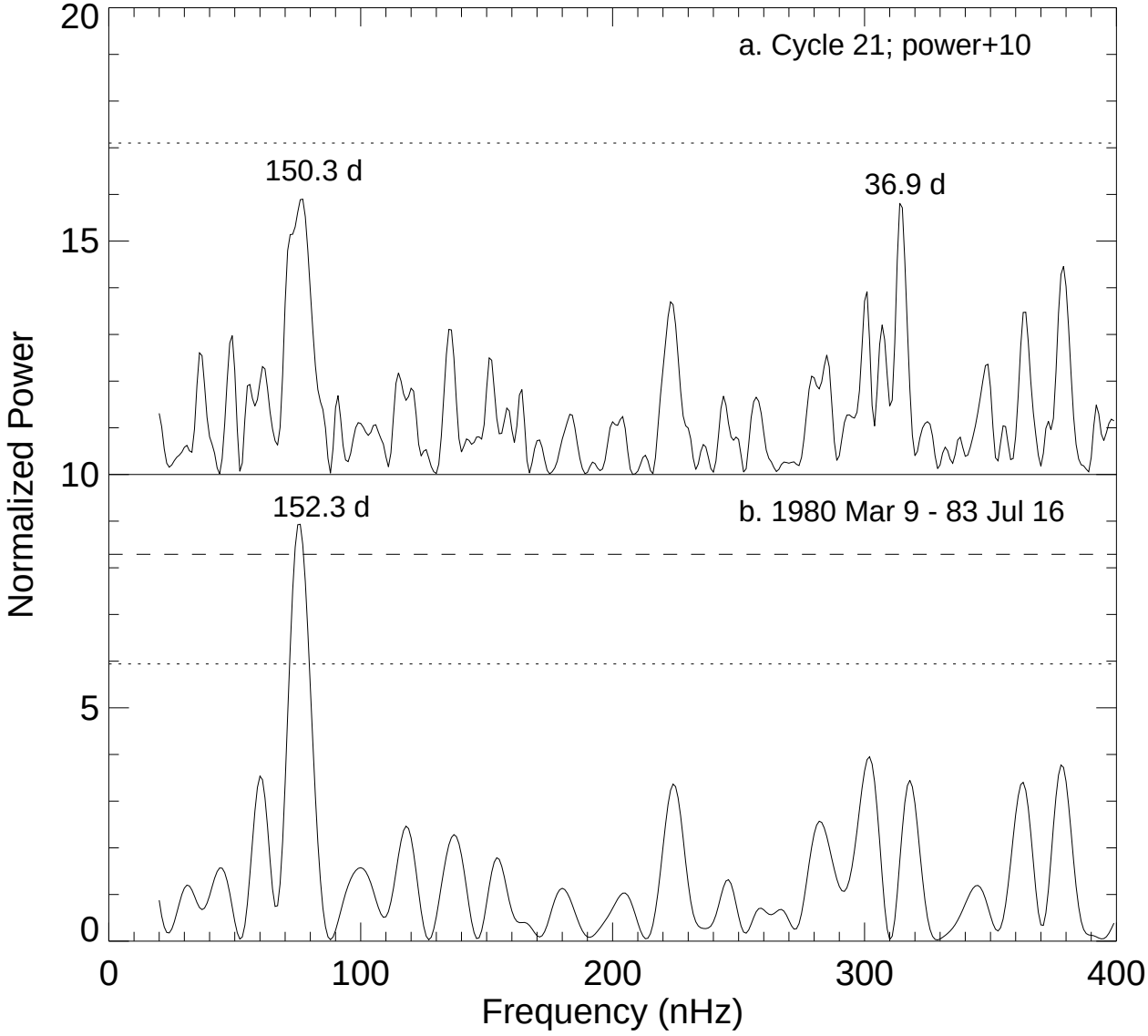

Fig. 11.— Power spectra for two time intervals of cycle 21. The first spectrum is for the entire cycle, and the second is for the interval when the 153-*d* periodicity was active. FAP levels of 10% and 1% are indicated as in the previous figure.

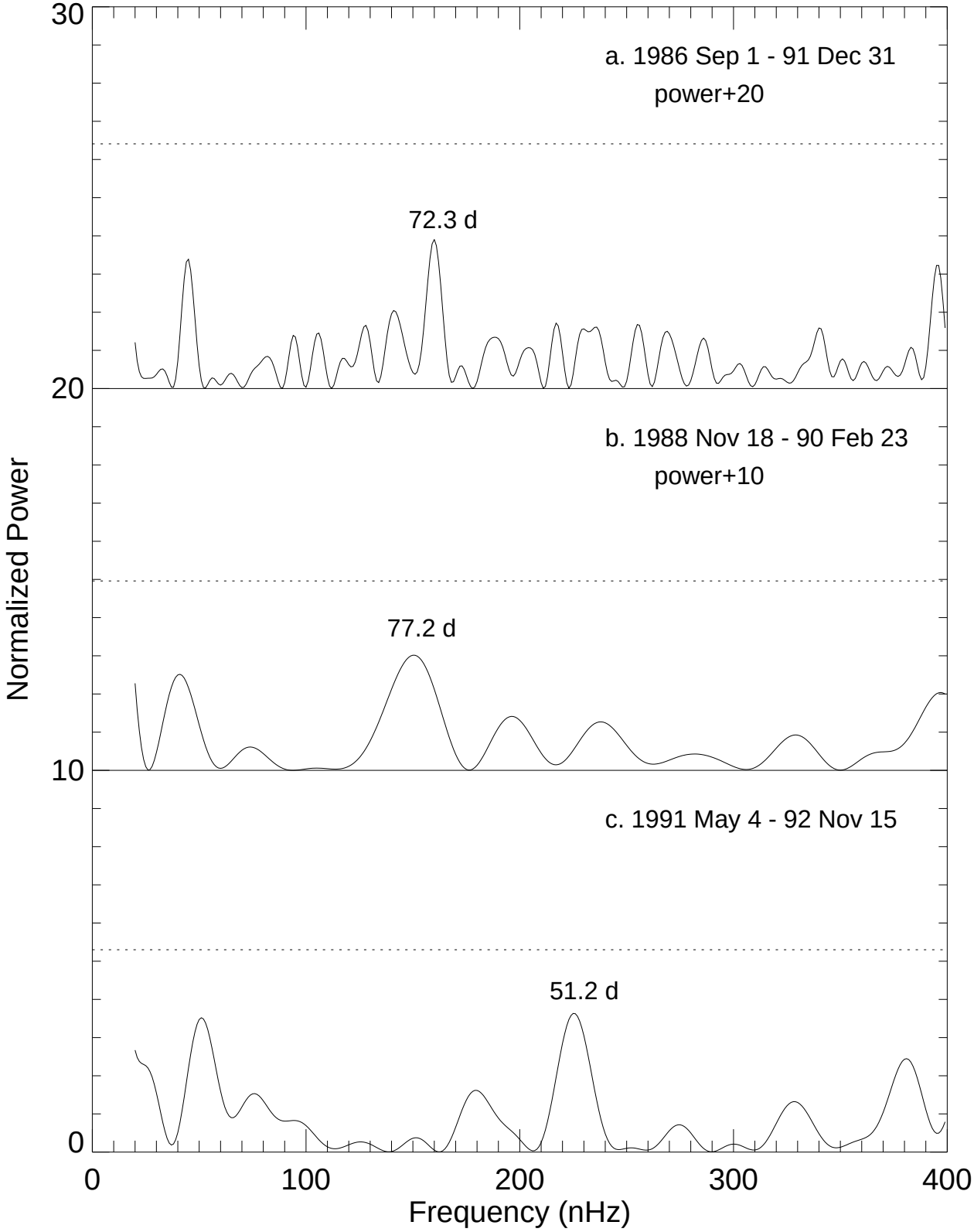

Fig. 12.— Power spectra for three intervals of cycle 22. No peaks are above the FAP level of 10%, shown by dotted lines.